Construction and Implementation Consideration of High-Frequency High-Efficiency RDCXs with Series-Parallel Two-Port Auxiliary Network

Tianji Liu, Xinke Wu, *Member, IEEE*

***Abstract*—In recent years, high-frequency high-efficiency DC/DC converters become popular in various applications. While conventional DC transformer (DCX) can achieve very high efficiency at high switching frequency, they are unable to realize voltage regulation due to the fixed switching frequency and duty cycle. To overcome this limitation while maintaining the benefits of DCX, a few partial-power-processing converters based on DCX have been invented for some applications. However, due to the absence of construction method for these regulated DCX (RDCX) converters, their topology types are limited and unable to fulfill the requirements of various applications. In this paper, a general method to construct RDCX by utilizing two-port auxiliary network is proposed. According to this method, some new RDCX topologies are derived and a family of high-frequency high-efficiency RDCXs is constructed to meet the requirements of more applications. To make full use of these RDCX topologies, their implementation consideration is discussed in detail and the characteristics of their suitable applications are summarized.**

***Index Terms*—DCX, partial-power processing, two-port auxiliary network, regulated DCX (RDCX)**

I. Introduction

Recently, there has been a growing demand for isolated DC-DC converters with high efficiency and power density in various applications [1], [2]. One effective way to increase power density is to increase the switching frequency, which reduces the size of passive components. Resonant converters can achieve high efficiency at high switching frequency due to their soft switching capability [3]-[5]. However, due to the conventional pulse-frequency modulation (PFM) control scheme, the switching frequency range of resonant converters expands with the increase of their resonant frequency to achieve voltage regulation. When the resonant frequency increases to several kilohertz (kHz) or even megahertz (MHz), the very wide switching frequency range will lead to great difficulties in magnetic components optimization [6]-[8], high-frequency control strategy [9]-[11] and synchronous rectifier (SR) driving [12]-[14], which make it hard to optimize the high-frequency PFM resonant converters.

Compared with the PFM resonant converter, DC transformer (DCX) based on resonant topology can avoid the challenges caused by wide switching frequency range due to fixed switching frequency and duty cycle. And this makes the DCX converters can be optimized to achieve extremely high efficiency even at MHz level switching frequency [15]-[18]. However, the constant voltage gain of the DCXs limits their use in applications requiring voltage regulation.

To maintain the benefits of DCX in applications requiring voltage regulation, some partial-power-processing converters based on DCX have been invented [19]-[28]. In these converters, additional auxiliary circuits are utilized to realize voltage regulation by handling a small portion of power, while most of the power is transferred by DCXs working at their optimal points for high efficiency.

In [19], the input terminals of auxiliary circuit and DCX are series connected, and the output terminals of them are parallel connected. Through undertaking the input voltage variation by the input terminal of auxiliary circuit, the input voltage of DCX is kept constant and the output voltage is regulated. Due to the input-series-output-parallel structure and this voltage regulation method, this converter can realize high-efficiency high-frequency power conversion in applications with low output voltage and high load current, such as telecom applications. Instead of series connecting the input of auxiliary circuit to the input of DCX, the primary winding of auxiliary transformer is series connected to the primary winding of main transformer to undertake the voltage variation in [20]. In [21]-[23], the output of the auxiliary circuit is series connected to the source to compensate the input voltage variation and realize voltage regulation. These converters can achieve higher efficiency in applications with nominal input voltage closer to the upper limit of input voltage range. In [24] and [25], series connecting the output of auxiliary circuit to the output of DCX makes it easy to achieve high efficiency in applications with high output voltage and wide output voltage range, such as electric vehicle (EV) chargers. In [26]-[28], current-fed resonant DCX are applied in the converters making them suitable for applications requiring less input-current ripple. Although these partial-power-processing regulated DCX (RDCX) converters can achieve high-frequency high-efficiency power conversion in some applications by their special design auxiliary circuits, the absence of a general construction method for RDCX makes their topology types limited to meet the requirements in numerous applications preferring high-frequency high-efficiency power conversion.

In this paper, by revealing the voltage regulation mechanism of current RDCX converter, a general construction method for high-frequency high-efficiency RDCX is presented. According to this method, some new RDCX topologies are derived, a family of RDCX topologies is constructed, and the requirements of more applications can be fulfilled. Moreover, to make full use of these topologies, their implementation consideration is also discussed in detail.

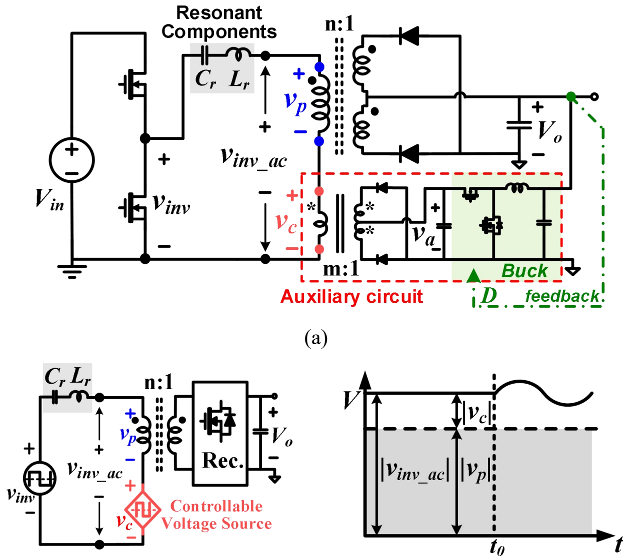

Fig. 1 RDCX proposed in [20]: (a) topology; (b) simplified circuit; (c) voltage regulation principle.

II. Derivation of RDCXs with Series Connected Controllable Voltage Source

A. An RDCX with Controllable Voltage Source Series Connected to Primary Winding

To realize high-efficiency high-frequency power conversion in step-down high-load-current applications requiring voltage regulation and galvanic isolation, an RDCX converter was proposed in [20]. As shown in Fig. 1(a), this RDCX is composed of DCX and auxiliary circuit. By adjusting D (duty cycle of the Buck converter), v_a and and $|v_c|$ (amplitude of v_c) is controlled, which makes the auxiliary circuit operates as a controllable voltage source. As the simplified circuit depicted in Fig. 1(b), this controllable voltage source is utilized to keep $|v_p|$ (amplitude of v_p) constant to realize output voltage regulation. Moreover, since the total voltage across the resonant components in DCX is almost zero, because of the fixed switching frequency neighboring the resonant frequency, v_{inv_ac} always equals to v_{inv}. Thus, the relationship among $|v_c|$, $|v_p|$ and $|v_{inv}|$ (amplitude of v_{inv}) and the voltage regulation principle can be illustrated in Fig. 1(c).

As presented in Fig. 1, due to the series connection of v_c and v_p, the ratio of the power processed by the auxiliary circuit P_{aux} to the power transferred to the load P_{Load}, is determined by the voltage ratio of v_c to V_{in}, as expressed in (1)

$$\frac{P_{aux}}{P_{Load}} = \frac{|v_c|}{|v_{inv\_ac}|} \tag{1}$$

Considering the voltage regulation principle of the RDCX, since v_c is employed to undertake the voltage variation in v_{inv_ac} to keep $|v_p|$ constant, $|v_c|$ is always far less than $|v_{inv\_ac}|$ during normal operation. Therefore, only a small fraction of power needs to be managed by the auxiliary circuit for voltage regulation in the RDCX converter.

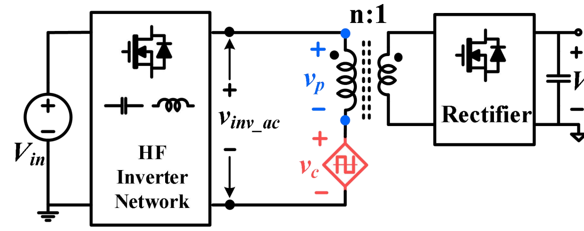

Fig. 2 Another simplified circuit of RDCX in Fig. 1.

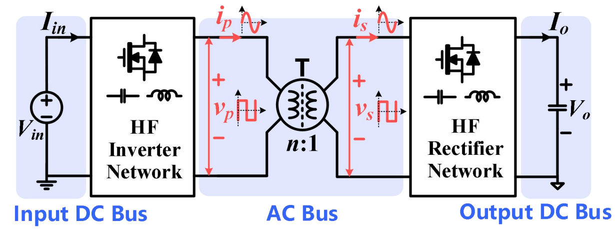

Fig. 3 Simplified circuit of resonant DCXs.

According to the operation principle of this RDCX, another simplified circuit can be derived in Fig. 2. In Fig. 2, since the total voltage across resonant components is almost zero, the primary-side switches and the resonant components are combined as a primary-side high-frequency (HF) inverter network, whose output AC voltage amplitude is in a fixed proportion to V_{in}.

B. Voltage Regulation of DCX through Series Connecting Controllable Voltage Source to Its Voltage Buses

To further explore the construction method of RDCX converters, the characteristics of the resonant DCXs should be considered at first. Since resonant components are also introduced to the secondary side and operates neighboring their resonant frequency in some two-direction resonant DCXs, such as CLLC-DCX, the resonant components and the switches at secondary side can also be combined as a high-frequency rectifier network [29]. Thus, according to the topologies and operation principles of the resonant DCX converters, a simplified circuit of resonant DCX can be derived in Fig. 3 [29]-[31].

In Fig. 3, according to the operation principles of resonant DCXs, the ratios between any two of V_{in}, V_o, $|v_p|$ (amplitude of v_p) and $|v_s|$ (amplitude of v_s) are each fixed. By extending the idea shown in Fig. 2, an auxiliary controllable voltage source can be connected in series to any bus of DCX to achieve voltage regulation. Following this idea, several simplified RDCX circuits can be derived, as shown in Fig. 4.

In Fig. 4(a), a controllable AC voltage source v_{cac} is connected in series to the primary side of the AC voltage bus to regulate the amplitude of AC-bus voltage. Besides the simplified circuit presented in Fig. 4(a), the controllable AC voltage source can also be connected to the secondary side of the AC voltage bus, which is not reiterated here. In Fig. 4(b) and (c), a controllable DC voltage sources v_{cdc} is connected in series to the input or output DC bus to accomplish voltage regulation by adjusting its DC value.

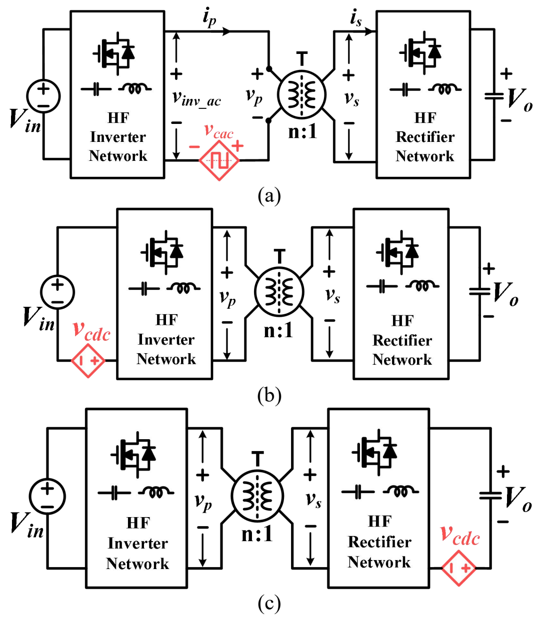

Fig. 4 Simplified circuits of RDCX converters with controllable voltage source series connected to voltage buses: (a) series connected to AC bus; (b) series connected to input DC bus; (c) series connected to output DC bus.

In Fig. 4, since v_{cdc} or v_{cac} are also utilized to compensate for bus voltage variations, their DC value or amplitude of AC value is usually smaller than that of the corresponding voltage bus during normal operation. Therefore, considering the series connection between controllable voltage source and the buses of DCX, only a small portion of power will be managed by the auxiliary controllable voltage sources in Fig. 4.

C. Controllable Voltage Source Realized by Series-Parallel Connected Two-Port Auxiliary Switching Network

Since there is a small portion of power managed by controllable voltage sources for voltage regulation in the RDCXs shown in Fig. 4, multi-port auxiliary switching networks should be employed to achieve power balance. Although auxiliary switching networks with three or more ports can also be applied [27], [28], their complex topology and large number of devices are easy to result in higher loss compared with the auxiliary networks only have two ports. Thus, in applications asking for high-frequency high-efficiency power conversion, two-port auxiliary switching networks are more preferred to realize the controllable voltage sources.

As presented in Fig. 5, the port v_{cdc} or v_{cac} should be connected in series to a voltage bus of the DCX, functioning as a controllable voltage source, while the other port v_x can be

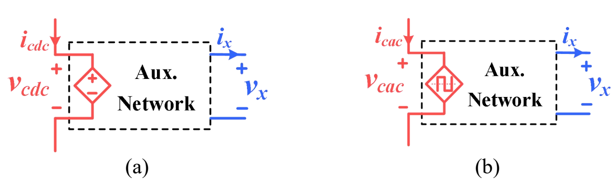

Fig. 5 Controllable voltage source realized by two-port auxiliary switching network: (a) DC source; (b) AC source.

It is important to note that voltage regulation cannot be realized when port v_x is also connected in series to the voltage bus of DCX. When the port v_x is connected in series to the voltage bus of DCX, the output voltage adjustment caused by regulating the voltage of port v_{cdc} (or v_{cac}) will be counteracted by the output voltage variation caused by the voltage change in port v_x. Thus, the output voltage is unable to be regulated by adjust the voltage of port v_{cdc} (or v_{cac}). When the port v_x is parallel connected to the voltage bus of DCX, the voltage regulation can be achieved. It is because the variation of the voltage of port v_{cdc} (or v_{cac}) only leads to change in i_x. The output voltage variation only caused by the voltage adjustment in port v_{cdc} (or v_{cac}). Thus, the two-port auxiliary networks in Fig. 5 should be series-parallel connected to any two of the voltage buses in DCX to operate as the controllable voltage source shown in Fig. 4.

When the two ports of the auxiliary network are connected to the same DC voltage bus, the entire circuit will become a two-stage circuit, in which a non-isolated DC/DC is cascaded to a resonant DCX. These converters are mainly used in photovoltaic and energy storage application [32]-[34], and will not discussed in this paper. Additionally, when the two ports of the auxiliary network are connected to the AC voltage bus, its topology will be very complicated and not suitable for high-frequency high-efficiency applications. Thus, according to the analysis above, eight RDCX structures can be derived by series-parallel connecting the two ports of the auxiliary network to different buses of the resonant DCX.

In Fig. 6, besides the port v_{cac} series connected to the primary-side AC voltage bus, the port v_{cac} series connected to the secondary-side AC voltage bus is also considered. Some of these structures in Fig. 6 have been applied in previously published partial-power-processing converters [19]-[28].

III. Implementation Considerations of RDCXs

To construct an RDCX based on the structures in Fig. 6, the topologies of two-port auxiliary networks should be discussed. Due to the different positions of the port v_{cdc} (or v_{cac}) and the port v_x in Fig. 6, the simplified circuits of the auxiliary networks can be classified and presented in Fig. 7.

In Fig. 7(a), the simplified circuit of the auxiliary networks with port v_{cac} series connected to the AC voltage bus and port v_x parallel connected to a DC voltage bus is displayed. In the simplified circuit, an AC-DC (A2D) network is employed for AC-DC conversion, and a non-isolated DC-DC (D2D) is utilized to adjust v_a to achieve voltage regulation. To attain isolation in the auxiliary network for normal operation, an auxiliary transformer is adopted. Similar to the converter displayed in Fig. 1, the A2D operate as part of the resonant DCX with its switching frequency f_{dcx}, while the non-isolated D2Ds are all independent of DCX, which can operate at a lower frequency to reduce its losses.

In the simplified circuit shown in Fig. 7(b), a frequency-independent non-isolated D2D is also used to realize voltage regulation and the D2A cooperating with DCX are also applied. Similar to Fig. 7(a), the port v_x should be isolated to

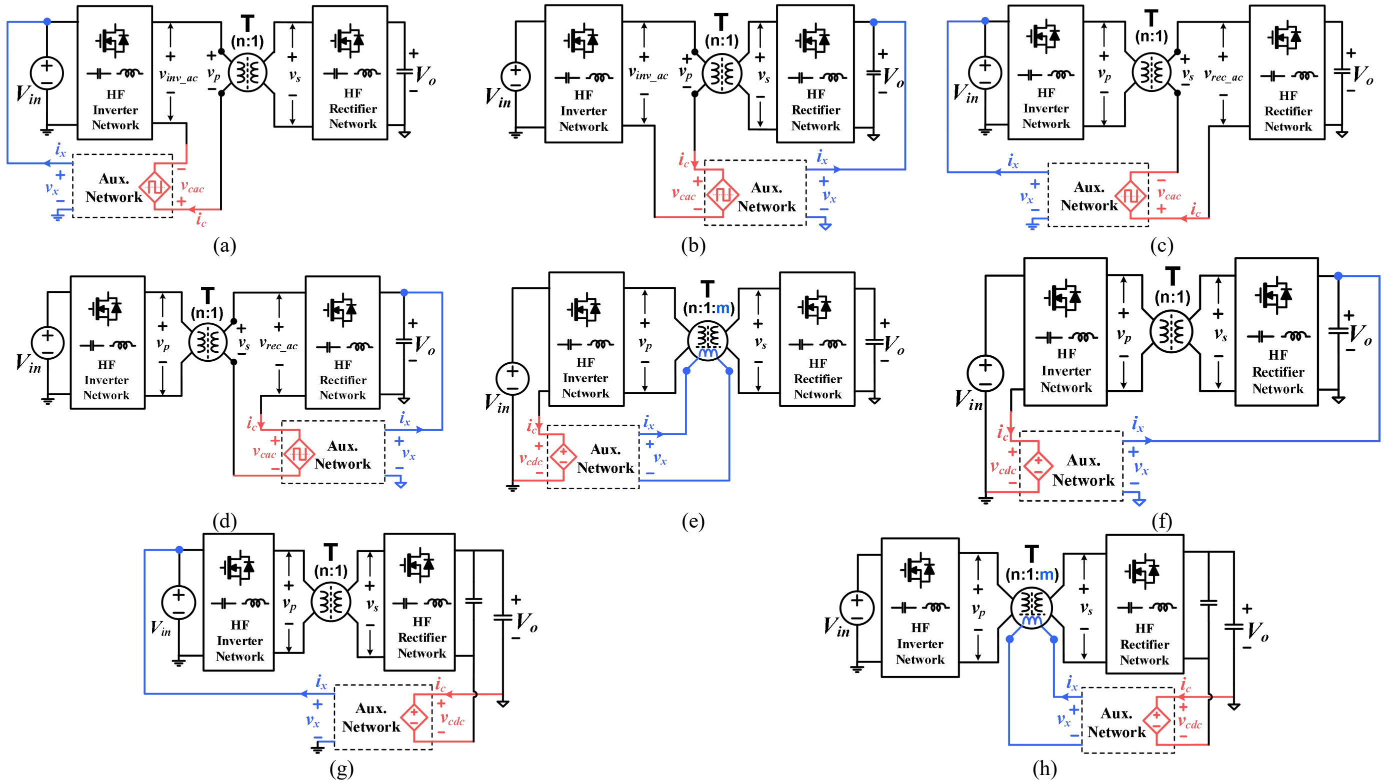

Fig. 6 Eight structures of RDCX with v_{cdc} (or v_{cac}) and v_x series and parallel connected to: (a) primary-side AC bus and input DC bus respectively; (b) primary-side AC bus and output DC bus respectively [20]; (c) secondary-side AC bus and input DC bus respectively; (d) secondary-side AC bus and output DC bus respectively; (e) input DC bus and AC bus respectively [21]-[23], [35]; (f) input DC bus and output DC bus respectively [19]; (g) output DC bus and input DC bus respectively [24], [25]; (h) output DC bus and AC bus respectively [26].

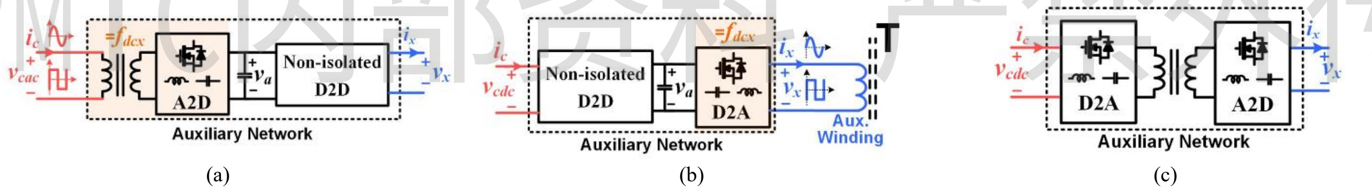

Fig. 7 Simplified topologies of auxiliary networks for RDCXs: (a) with v_{cac} series connected to the AC bus and v_x parallel connected to the DC bus; (b) with v_{cdc} series connected to the DC bus and v_x parallel connected to the AC bus; (c) with v_{cdc} and v_x connected to the DC buses.

the AC voltage bus of DCX for normal operation. By utilizing an auxiliary winding, the isolation is realized without introducing an additional auxiliary transformer.

In Fig. 7(c), when v_{cdc} and v_x are connected to the DC voltage buses, the auxiliary network should be an isolated D2D converter which composed of a D2A network, an auxiliary transformer and a A2D network. Since both v_{cdc} and v_x are coupled with DCX at DC buses, the topology, switching frequency, and control strategy of this isolated D2D are independent from the DCX.

To achieve high overall efficiency in RDCXs, the losses produced by the auxiliary network should be reduced. In order to reduce the losses of the auxiliary network, the power dealt by it should be reduced and the its operation efficiency needs to be improved.

A. Reduce the Power Dealt by the Auxiliary Network

To estimate the power dealt by the auxiliary network, a coefficient K_{aux} ($=P_{aux}/P_{dcx}$) can be defined. Due to the series connection of the port v_{cdc} (or v_{cac}) and a voltage bus of DCX, K_{aux} can be decreased by reducing v_{cdc} or $|v_{cac}|$ (amplitude of v_{cac}). Thus, to attain high overall efficiency in RDCX, v_{cdc} or $|v_{cac}|$ should be diminished in the normal operation.

In the RDCX architectures illustrated in Fig. 6, if the v_{cdc} is positive or the phase of v_{cac} is aligned with that of v_p, the relationships between K_{aux} and V_{in}, and K_{aux} and V_o can be derived in Figures 8(a) and (b) respectively. As shown in Fig. 8(a), when V_o is constant, lower V_{in} will result in lower K_{aux}. In Fig. 8(b), when V_{in} is constant, higher V_o will result in higher K_{aux}. Thus, by reducing P_{aux} at nominal operation point, the RDCX structures with positive v_{cdc} or v_{cac} are more suitable for applications with nominal input voltage V_{inN} near their lower limit of input voltage range or nominal output voltage V_{oN} near their upper limit of output voltage range. As shown in Fig. 8(c) and (d), the curves of K_{aux} can be derived with negative polarity of v_{cdc} or v_{cac}, which means a negative value of v_{cdc} or the phase of v_{cac} opposite to that of v_p. According to Fig. 8(c) and (d), it can be known that in application with nominal input voltage near their upper limit of input voltage range or

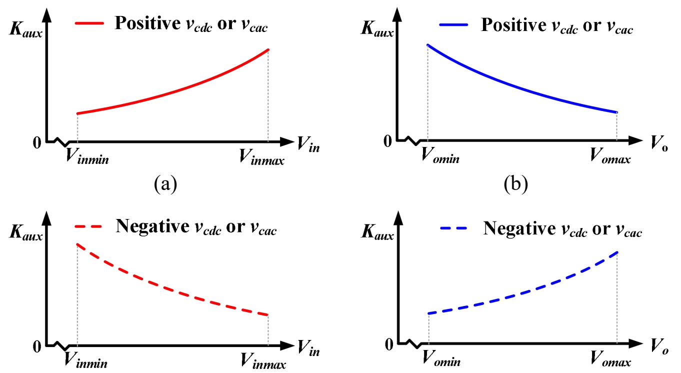

Fig. 8 K_{aux} curve with variation in V_{in} or V_o: (a) K_{aux} vs. V_{in} with positive v_{cdc} or v_{cac}; (b) K_{aux} vs. V_o with positive v_{cdc} or v_{cac}; (c) K_{aux} vs. V_{in} with negative v_{cdc} or v_{cac}; (d) K_{aux} vs. V_o with negative v_{cdc} or v_{cac}.

nominal output voltage near their lower limit of the output voltage range, the polarity of v_{cdc} or v_{cac} in the RDCX structures should be negative to reduce P_{aux}. Moreover, no matter the polarity of the port v_{cdc} (or v_{cac}), the voltage regulation in the RDCX structures shown in Fig. 6 will not be affected.

In the RDCX architectures illustrated in Fig. 6, if the v_{cdc} is positive or the phase of v_{cac} is aligned with that of v_p, the relationships between K_{aux} and V_{in}, and K_{aux} and V_o can be derived in Figures 8(a) and (b) respectively. As shown in Fig. 8(a), when V_o is constant, lower V_{in} will result in lower K_{aux}. In Fig. 8(b), when V_{in} is constant, higher V_o will result in higher K_{aux}. Thus, by reducing P_{aux} at nominal operation point, the RDCX structures with positive v_{cdc} or v_{cac} are more suitable for applications with V_{inN} near their lower limit of input voltage range or V_{oN} near their upper limit of output voltage range.

As shown in Fig. 8(c) and (d), the curves of K_{aux} can be derived with negative polarity of v_{cdc} or v_{cac}, which means a negative value of v_{cdc} or the phase of v_{cac} opposite to that of v_p. According to Fig. 8(c) and (d), it can be known that in application with V_{inN} near their upper limit of input voltage range or V_{oN} near their lower limit of the output voltage range, the polarity of v_{cdc} or v_{cac} in the RDCX structures should be negative to reduce P_{aux}. Moreover, no matter the polarity of the port v_{cdc} (or v_{cac}), the voltage regulation in the RDCX structures shown in Fig. 6 will not be affected.

As shown in Fig. 9(a), a 380V/336V RDCX converter based on the structure in Fig. 6(c) for high-voltage DC power supply is presented. Since the nominal output voltage is around 380V which is close to the upper limit of the output voltage range (270V-400V). Thus, the polarity of port v_{cac} is designed to be positive, and K_{aux} is reduced to around 10% at its nominal output voltage. The auxiliary network of this RDCX employs a high-frequency rectifier operating at the DCX switching frequency f_{dcx} to generate a controllable AC voltage source. The operation principle of this RDCX is validated through simulation, as shown in Fig. 9(b) and (c). In Fig. 9(b), zero-voltage-switching (ZVS) turn on is achieved in Q_1-Q_4, reducing their switching loss. Fig. 9(c) demonstrates voltage regulation. As V_{in} varies, the duty cycle D of the auxiliary Boost converter (represented by the driving signal G_a) is

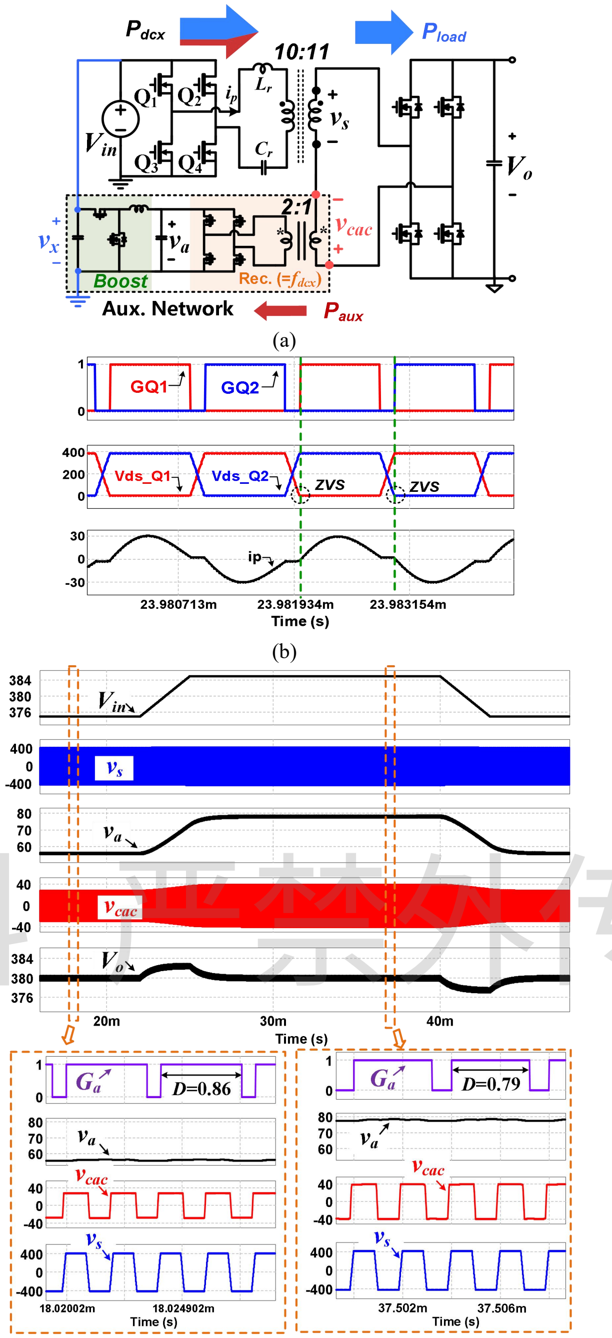

Fig. 9 A 380V/336V RDCX converter based on the structure in Fig. 6(c) with positive v_{cac}: (a) topology; (b) ZVS operation of Q_1-Q_4 with 380Voutput and full load; (c) voltage regulation with a step change in V_{in}.

adjusted, and the $|v_{cac}|$ is regulated to undertake the variation of v_s to keep $|v_{rec\_ac}|$ constant and achieve output voltage regulation.

In Fig. 10(a), a 48V-400V RDCX converter also based on the structure in Fig. 6(c) is depicted. In this converter, since the nominal input voltage is around 55V, which is close to its upper limit of the input voltage range (40V-60V), v_{cac} is designed to be negative to minimize P_{aux} at its nominal input voltage (~55V). Thus, at the nominal input voltage, K_{aux} is around 17.5%. The auxiliary network is a high-frequency

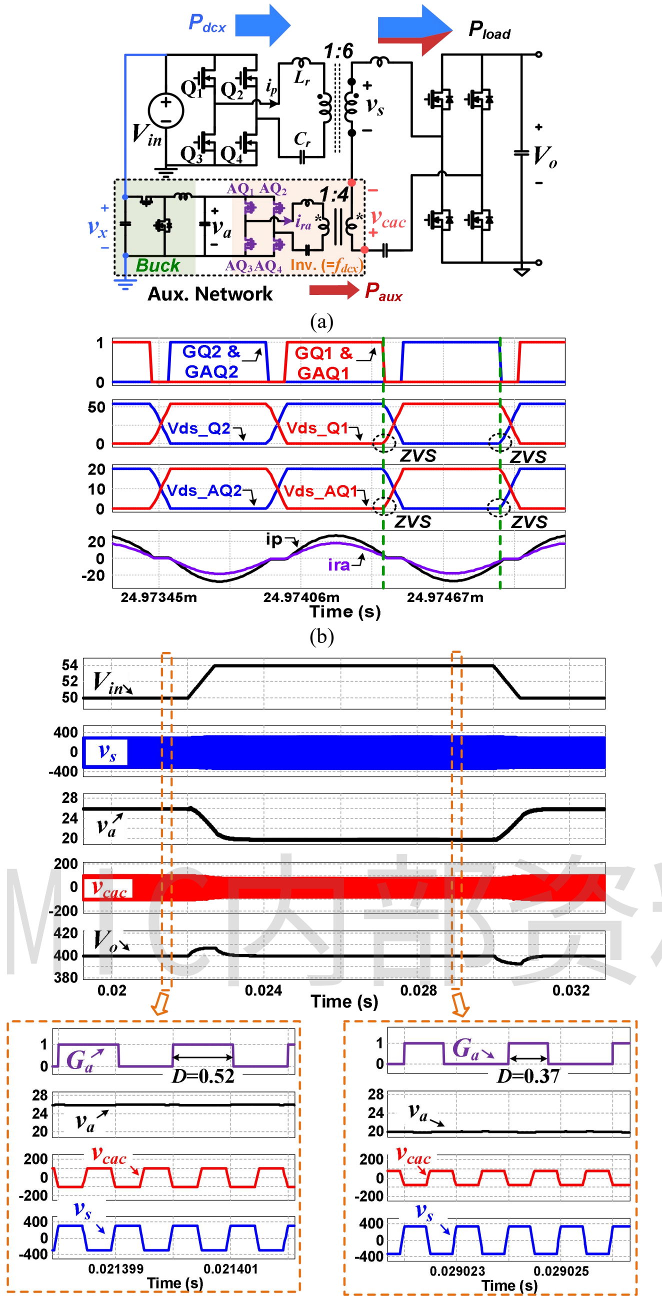

(c)

Fig. 10 A 48V/400V RDCX converter based on the structure in Fig. 6(c) with negative v_{cac}: (a) topology; (b) ZVS operation of Q_1-Q_4 and AQ_1-AQ_4 at full load; (c) voltage regulation with a step change in V_{in}.

inverter operating at the DCX switching frequency f_{dcx} to generate a controllable AC voltage source. Fig. 10(b) illustrates the ZVS turn on of Q_1-Q_4 and AQ_1-AQ_4. In Fig. 10(c), by controlling the duty cycle D of the auxiliary Buck converter, $|v_{cac}|$ is adjusted to compensate the variation in v_s, maintaining the regulated output voltage.

B. Reduce the Losses Produced by DCX

The two examples above shows that in applications with nominal voltage near the upper or lower limits of the voltage range, the polarity of v_{cdc} or v_{cac} can be easily determined to reduce K_{aux}. However, in applications with nominal voltage in the middle of the voltage range, the power dealt by the auxiliary networks remains almost the same no matter the polarity of the port v_{cdc} (or v_{cac}). In this situation, the power flow direction in the auxiliary circuit should be considered. In the RDCX structures shown in Fig. 6, different v_{cdc} (or v_{cac}) polarities result in distinct P_{aux} power flow directions. In some conditions, the P_{aux} might be further processed by the DCX, as shown in Fig. 9(a), which will result in additional loss in DCX. Thus, when the polarity of v_{cdc} (or v_{cac}) does not significantly affect K_{aux}, the polarity without circulating P_{aux} is recommended for higher efficiency.

C. Improve the Efficiency of Auxiliary Networks

Besides reducing P_{aux} and eliminating the circulating power, enhancing the efficiency of the auxiliary network can further reduce the losses. Since v_{cdc} (or v_{cac}) is used to undertake or compensate the voltage variation of DCX voltage bus, the value of v_{cdc} (or $|v_{cac}|$) is small. To reduce the current stresses of the devices associating with port v_{cdc} (or v_{cac}) in the auxiliary network, the port v_{cdc} (or v_{cac}) should be series connected to the DCX buses with higher voltage and less current.

Moreover, due to the partial-power processing, the output current of the port v_x is small. In order to reduce the voltage stresses of devices associating with port v_x, the v_x should be parallel connected to the DCX buses with lower voltage. Furthermore, in structures shown in Fig. 6(e) and (h), by selecting the turn number of the auxiliary winding, the voltage of the port v_x can be optimally designed to reduce the voltage stresses.

Thus, according to the input and output voltage of applications, appropriate RDCX structures can be selected with low voltage and current stresses of devices in the auxiliary networks.

D. A Brief Comparison of the Volume of Auxiliary Networks

In some applications with stringent requirements on the volume of the converters, the size of the auxiliary network needs to be considered. The size of auxiliary network is mainly decided by the volume of its auxiliary transformer. Assuming the same operating frequency and power in the auxiliary transformers, a rough comparison of the auxiliary transformers can be made by considering their insulation requirements. The auxiliary transformers used for primary-secondary isolation will be larger than those for functional isolation. And, the auxiliary networks without auxiliary transformer will be the smallest. The insulation requirements of each RDCX structure in Fig. 6 is shown in Table I.

According to the analysis above, the characteristics of suitable applications and implementation considerations of each RDCX can be summarized and presented in Table I.

TABLE I CHARACTERISTICS OF SUITABLE APPLICATIONS AND IMPLEMENTATION CONSIDERATION OF RDCXS

Structure	Auxiliary network	Characteristics of preferred applications	Preferred polarity of v_{cac} (or v_{cdc}) according to the nominal voltage			Insulation requirement of auxiliary transformer
			V_{inN} close to V_{inmax} or V_{oN} close to V_{omin}	V_{inN} close to V_{inmin} or V_{oN} close to V_{omax}	V_{inN} or V_{oN} in the middle	
Fig. 6(a)	Fig. 7(a)	$V_{in} \approx V_o$	v_{cac} (or v_{cdc}) < 0	v_{cac} (or v_{cdc}) > 0	$v_{cac} < 0$	Functional insulation
Fig. 6(b)	Fig. 7(a)	$V_{in} \geqslant V_o$			$v_{cac} > 0$	Primary-secondary insulation
Fig. 6(c)	Fig. 7(a)	$V_{in} \leqslant V_o$			$v_{cac} < 0$	Primary-secondary insulation
Fig. 6(d)	Fig. 7(a)	$V_{in} \approx V_o$			$v_{cac} > 0$	Functional insulation
Fig. 6(e)	Fig. 7(b)	$V_{in} \geqslant V_o$			$v_{cdc} > 0$	-
Fig. 6(f)	Fig. 7(c)	$V_{in} \geqslant V_o$			$v_{cdc} > 0$	Primary-secondary insulation
Fig. 6(g)	Fig. 7(c)	$V_{in} \leqslant V_o$			$v_{cdc} < 0$	Primary-secondary insulation
Fig. 6(h)	Fig. 7(b)	$V_{in} \leqslant V_o$			$v_{cdc} < 0$	-

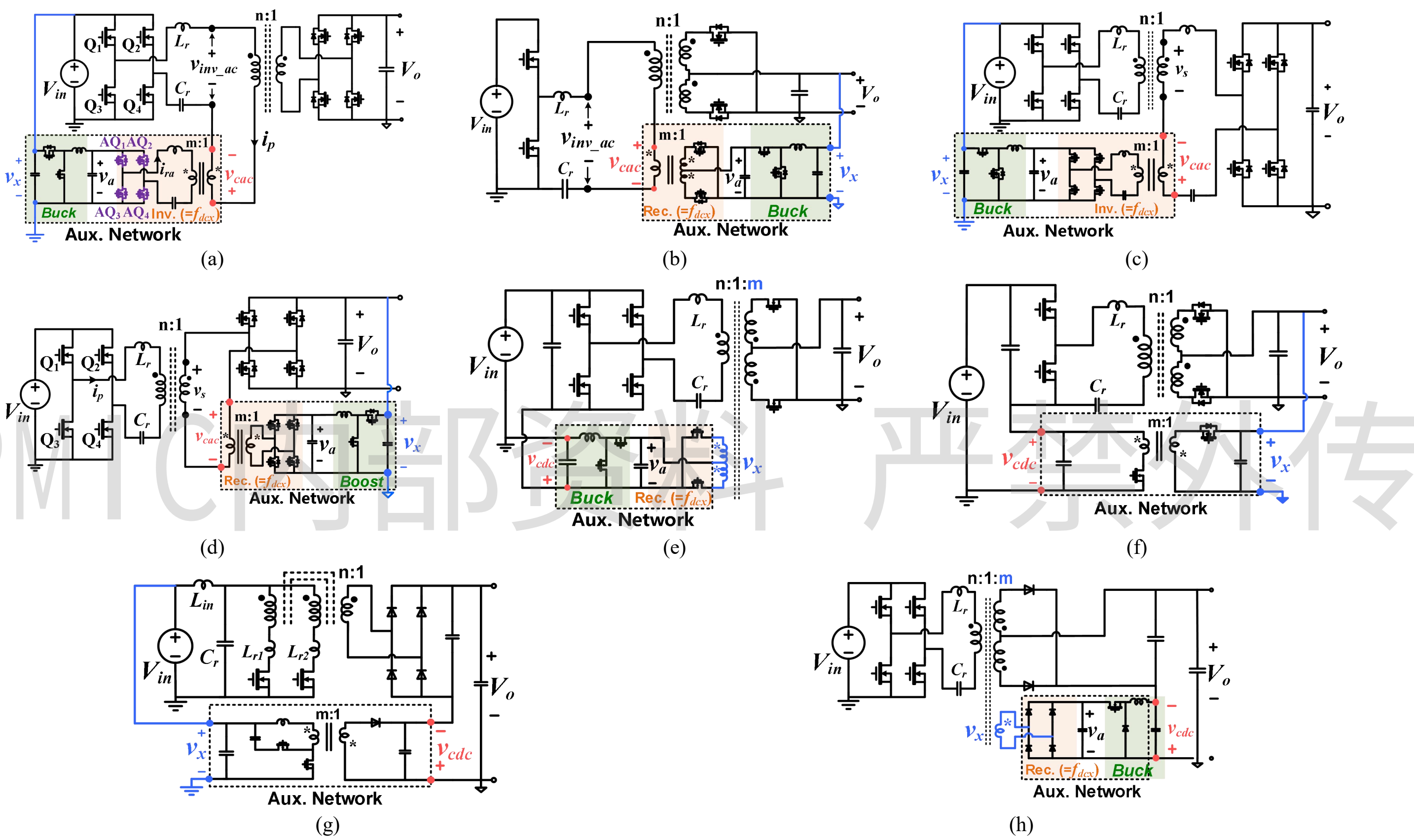

Fig. 11 Eight RDCX examples: (a) corresponding to Fig 6(a); (b) corresponding to Fig 6(b) [20]; (c) corresponding to Fig 6(c); (d) corresponding to Fig 6(d); (e) corresponding to Fig 6(e) [22]; (f) corresponding to Fig 6(f) [19]; (g) corresponding to Fig 6(g) [26]; (h) corresponding to Fig 6(h) [24].

IV. SIMULATION AND EXPERIMENTAL VERIFICATION

A. Simulation Verification

To verify the implementation consideration and operation principle of RDCXs based on Fig. 6 and Fig. 7, RDCX converter examples applied in appropriate applications, which match the summarized characteristics in Table I, are verified through simulation and experiments. In Fig. 11, eight RDCX examples are illustrated. Since the converters in Fig. 11(b), (e), (g), (f) and (h) are verified in former publications and the converter in Fig. 11(c) is validated by simulation shown in Fig. 10, the converters in Fig. 11(a) and (d) are verified in appropriating applications by simulation in this section.

In a two-stage on-board EV charger with 450V-850V output, its 2nd-stage DC/DC input voltage can be 550V-850V which increasing with output voltage linearly to improve the efficiency. In this case, the RDCX converter in Fig. 11(a) can be applied and the turn ratios of the main transformer and auxiliary transformer are 19:15 and 2:1, respectively. With the output voltage increasing from 450V to 850V, the K_{aux} increase from 7.4% to 21%, which means the power dealt by auxiliary network always less a quarter of the load power. Its operation is verified by the simulation shown in Fig. 12.

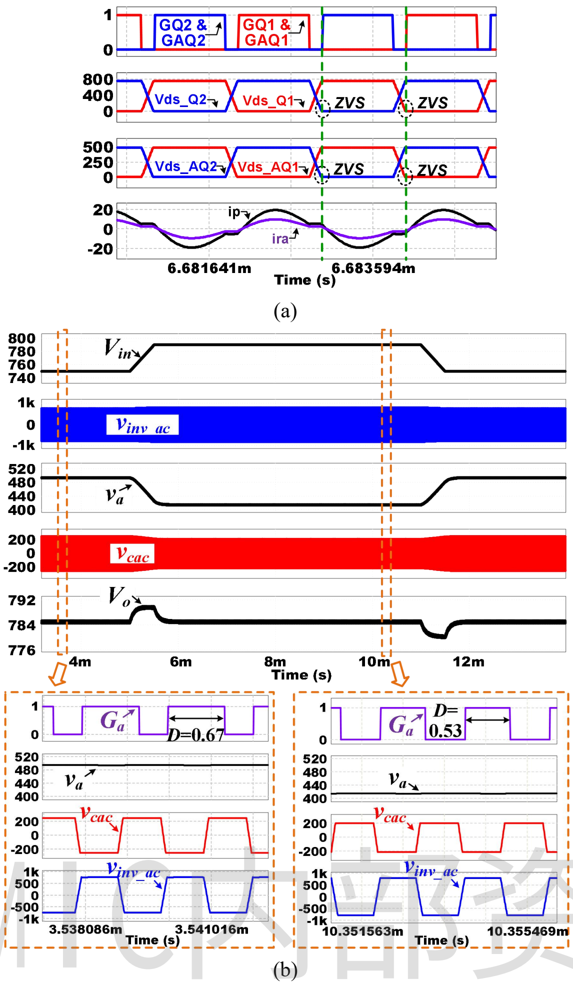

Fig. 12 Simulation of RDCX in Fig.11(a): (a) ZVS operation of Q_1-Q_4 and AQ_1-AQ_4 at full load; (b) voltage regulation with a step change in V_{in}.

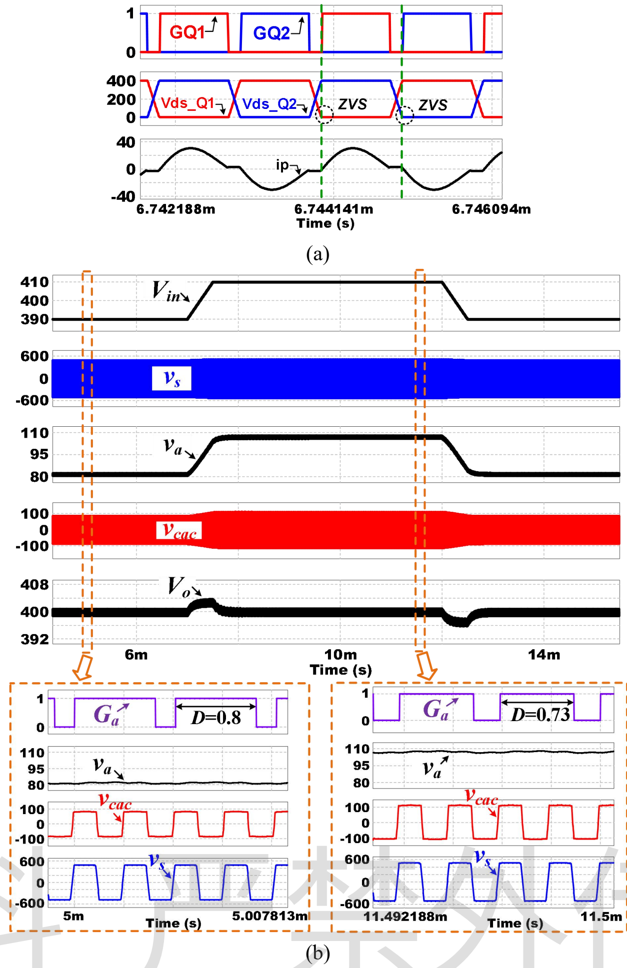

Fig. 13 Simulation of RDCX in Fig.11(d): (a) ZVS operation of Q_1-Q_4 at full load; (b) voltage regulation with a step change in V_{in}.

In another EV charger with 250V-450V output, the input voltage of the 2nd-stage is 400V. In this case the RDCX converter in Fig. 11(d) can be utilized. The turn ratios of the main transformer and auxiliary transformer are 4:5 and 1:1, respectively. Since the output voltage range is very wide, the polarity of port v_{cac} is designed to be negative to eliminate the circulating power. With the output voltage increasing from 250V to 450V, the power dealt by the auxiliary network is always less than half of the load power. Its operation principle is validated through simulation shown in Fig. 13.

B. A Prototype for Experimental Verification

In the two-stage multi-cell AC-DC converter, the 2nd-stage DC-DC converters require high-efficiency high-power-density power conversion and simple control strategy of bus-voltage balance [36]. However, they cannot be achieved simultaneously by conventional DC/DC topologies. Due to their high-frequency high-efficiency power conversion capability and the characteristics of PWM control, when an PWM D2D is applied in the auxiliary network, these two requirements can be easily obtained by applying the RDCX topologies [23].

In Fig.14(a), the simplified circuit of a 220Vac/48Vdc-3kW two-stage 6-cell AC-DC converter is presented. According to the summary shown in Table I, the appropriate RDCX topology can be derived. Since the average value of each DC-bus voltage V_{dci} is around 65V and V_o is 48V, the port v_{cac} (or v_{cdc}) should be series connected to the primary side. Thus, the RDCX structures shown in Fig. 6(a), (b), (e) and (f) can be selected. Considering the high requirement on power density, the structure shown in Fig. 6(e) is the best choice.

Furthermore, to choose the polarity of the port v_{cdc}, the turn ratio of the transformer is designed with minimized K_{aux} in different polarity. When the polarity of port v_{cdc} is negative, in order to realize output voltage regulation with V_{dci} varying between 59V-71V and minimize the K_{aux}, the turn ratio of primary winding to secondary winding is designed to be 3:2, and the K_{aux} is 10.8% at 65V V_{dci}; When the polarity of port v_{cdc} is positive, the turn ratio of primary winding to secondary winding should be 1:1 and the K_{aux} is 26.2% at 65V V_{dci}. Thus, the polarity is selected to be negative. Then, the turn ratio of transformer can be further designed to be 3:2:1 and a Buck converter is chosen to be the PWM D2D. The topology of this 2nd-stage DC-DC converter is shown in Fig. 14(b). The DC-bus voltage balance has already been discussed in [23].

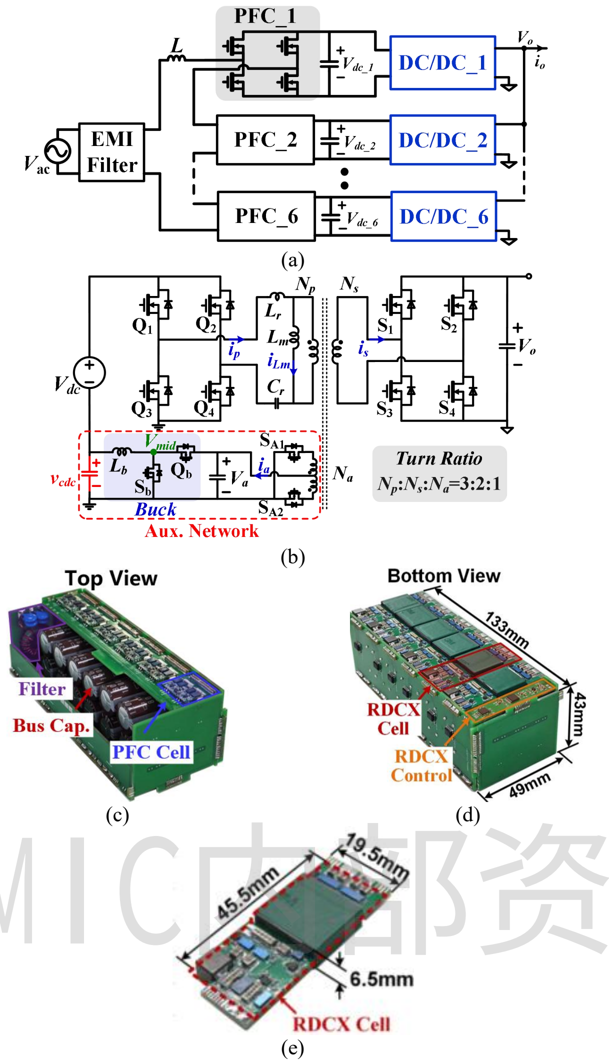

Fig. 14 Prototype of 6-cell AC-DC converter: (a) simplified circuit of 6-cell AC-DC; (b) topology of 2nd-stage RDCX cell; (c) top view of the AC-DC prototype; (d) bottom view of the AC-DC prototype; (e) prototype of a RDCX cell.

TABLE II KEY PARAMETERS OF A 2ND-STAGE RDCX CELL

Description	Parameters
Input	61V-69V
Output	48V/ 500W
Switching frequency	1MHz (DCX)/ 600kHz (Buck)
Q_1~Q_4	EPC2053
S_1~S_4	EPC2206
S_{A1} and S_{A2}	EPC2045
Switches in Buck	Q_b: EPC2015C S_b: EPC2030
Inductor L_b in Buck	XEL6060-272ME
Resonant components	C_r: 680nF; L_r: 26nH (leakage inductance)
Transformer	L_m: 5μH; Material: ML91S;

The prototype of the whole 6-cell AC/DC converter is presented in Fig. 14(c) and (d), and the prototype of a 2nd-stage RDCX converter based on Fig. 14(b) is shown in Fig. 14(e). According to the size shown in Fig. 14(e), the power density of the RDCX cell reaches around 1400W/in^3. The

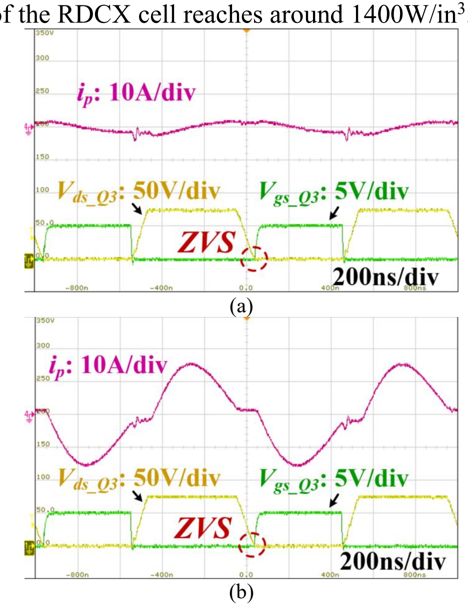

Fig. 15 ZVS operation of RDCX cell: (a) null load; (b) full load.

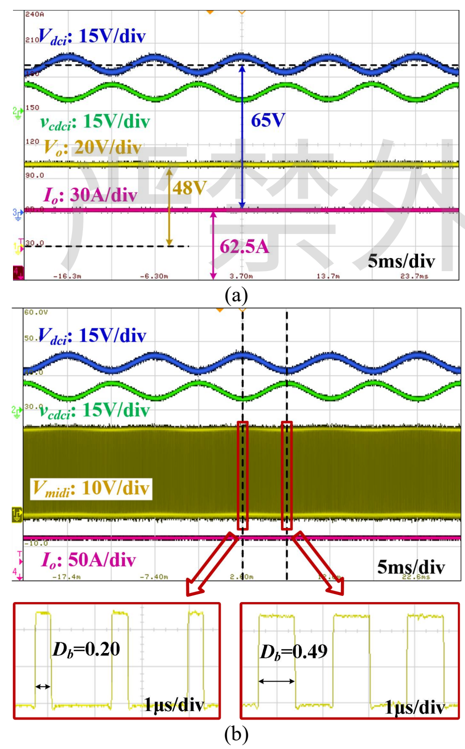

Fig. 16 Voltage regulation in the *i*th RDCX cell: (a) V_o and v_{cdc} waveforms; (b) v_{cdc} adjustment by varying the duty cycle of Buck D_b.

density of a RDCX cell reaches around 1400W/in^3. The parameters of the 2nd-stage RDCX cell is shown in Table II.

As shown in Fig. 15 the ZVS turn on of Q_3 can be achieved in null load and full load conditions. Thus, according to the operation principle of resonant DCX, ZVS turn on can be realized by Q_3-Q_4 in all load conditions.

In Fig. 16, the voltage regulation of the *i*th RDCX cell is presented. With twice-line-frequency voltage ripple in DC bus, output voltage is kept constant by adjusting the duty cycle of Buck converter D_{bi} to regulate v_{cdci}.

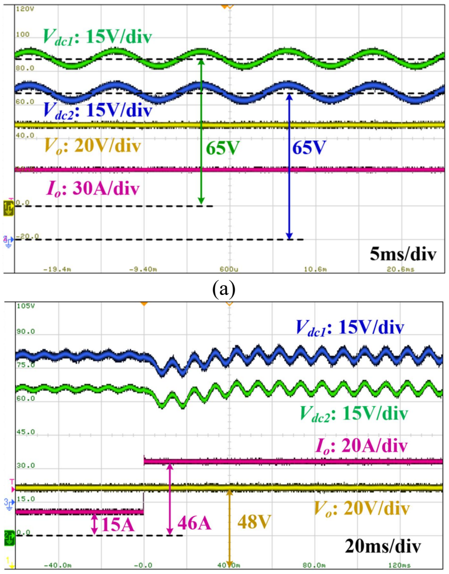

Fig. 17 DC-bus voltage sharing: (a) steady state at full load; (b) with load change from 25% to 75%.

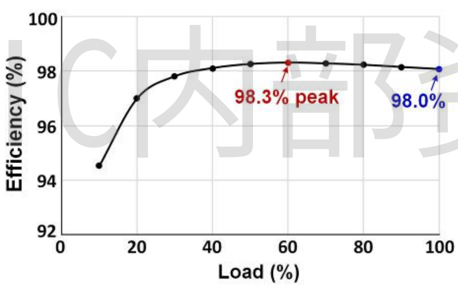

Fig. 18 Measured efficiency of RDCX cell.

In Fig. 17, the DC-bus voltage balance is illustrated. As shown in Fig. 17(a), the steady-state DC-bus voltage balance can be realized in full-load condition. As shown in Fig. 17(b), The dynamic-state DC-bus voltage balance can also be achieved even with a step change in load current from 25%-75%.

The measured efficiency of a RDCX cell is shown in Fig. 18. As shown in Fig. 18, the peak efficiency of the RDCX cell reaches 98.3% at around 60% load, and the efficiency at full load is around 98.0%.

According to the experiments, the summarized characteristics of applications suitable for each RDCX shown in Table I and the voltage regulation principle is verified in the two-stage 6-cell AC-DC application.

VI. Conclusion

By elucidating the voltage regulation mechanism of existing partial-power-processing converters, a general construction method for high-frequency, high-efficiency RDCX converters is proposed for applications that require isolated power conversion with voltage regulation capability. By this method, new RDCX topologies are derived and the application range of RDCX converters can be expanded.To make full use of the partial-power-processing ability of the RDCX converters, their implementation consideration is discussed in detail and the characteristics of applications suitable for each RDCX is summarized. The implementation consideration and the operation principle of these RDCXs are verified through simulation and experiments.

References

[1] International Energy Agency, Global EV Outlook. 2019. [Online]. Available: https://www.iea.org/reports/global-ev-outlook-2019

[2] Natural Resources Defense Council, “Data center efficiency assessment—Scaling up energy efficiency across the data center industry evaluating key drivers and barriers,” Aug. 2014. [Online]. Available: https://www.nrdc.org/sites/default/files/data-center-efficiency-assessment-IP.pdf

[3] R. P. Severns, "Topologies for three-element resonant converters", IEEE Trans. Power Electron., vol. 7, no. 1, pp. 89-98, Jan. 1992.

[4] Bo Yang, F. C. Lee, A. J. Zhang and Guisong Huang, "LLC resonant converter for front end DC/DC conversion," in Proc. IEEE Appl. Power Electron. Conf. Expo. (APEC), Dallas, TX, USA, Mar. 2002, pp. 1108-1112.

[5] W. Chen, P. Rong and Z. Lu, "Snubberless bidirectional DC–DC converter with new CLLC resonant tank featuring minimized switching loss", IEEE Trans. Ind. Electron., vol. 57, no. 9, pp. 3075-3086, Sep. 2010.

[6] M. H. Ahmed, A. Nabih, F. C. Lee and Q. Li, "Low-loss integrated inductor and transformer structure and application in regulated LLC converter for 48-V bus converter", IEEE Trans. Emerg. Sel. Topics Power Electron., vol. 8, no. 1, pp. 589-600, Mar. 2020.

[7] B. Li, Q. Li and F. C. Lee, "High-frequency PCB winding transformer with integrated inductors for a bi-directional resonant converter", IEEE Trans. Power Electron., vol. 34, no. 7, pp. 6123-6135, Jul. 2019.

[8] M. Li, Z. Ouyang and M. A. E. Andersen, "High-Frequency LLC Resonant Converter With Magnetic Shunt Integrated Planar Transformer," IEEE Trans. Power Electron., vol. 34, no. 3, pp. 2405-2415

[9] Z. Hu, Y.-F. Liu and P. C. Sen, "Bang-bang charge control for LLC resonant converters", IEEE Trans. Power Electron., vol. 30, no. 2, pp. 1093-1108, Feb. 2015.

[10] C. Fei, F. C. Lee and Q. Li, "Multi-step Simplified optimal trajectory control (SOTC) for fast transient response of high frequency LLC converters", Proc. IEEE Energy Convers. Congr. Expo., pp. 2064-2071, 2015.

[11] J. Zhao et al., "Fast and Accurate Control Strategy for LCC Resonant Converters Based on Simplified State Trajectory and Two-Point Solution Method," IEEE Trans. Power Electron., vol. 37, no. 5, pp. 5309-5319, May 2022.

[12] D. Wang and Y. Liu, " A zero-crossing noise filter for driving synchronous rectifiers of LLC resonant converter ", IEEE Trans. Power Electron., vol. 29, no. 4, pp. 1953-1965, May 2014.

[13] J. D. Hsu, M. Ordonez, W. Eberle, M. Craciun and C. Botting, " LLC synchronous rectification using resonant capacitor voltage ", IEEE Trans. Power Electron., vol. 34, no. 11, pp. 10970-10987, Feb. 2019.

[14] L. Pei et al., "A Time-Domain-Model-Based Digital Synchronous Rectification Algorithm for CLLC Resonant Converters Utilizing a Hybrid Modulation," IEEE Trans. Power Electron., vol. 37, no. 3, pp. 2815-2829, Mar. 2022.

[15] G. Li and X. Wu, "A 98.4% Efficiency 380V-12V DCX with 1.3kW/in3 Power Density Using Low NFoM Devices and Resonant Drive Transformer," IEEE Trans. Power Electron., vol. 37, no. 10, pp. 12346-12356, Oct. 2022.

[16] MPC1100A-54 Datasheet. (2021, Mar.). 300W Fixed Ratio Digital DC/DC Power Module [Online]. Available: https://www.monolithicpower.cn/cn/documentview/productdocument/i

ndex/version/2/document_type/Datasheet/lang/en/sku/MPC1100A-54-0000/document_id/9431/
[17] M. H. Ahmed, F. C. Lee and Q. Li, "Two-stage 48-V VRM with intermediate bus voltage optimization for data centers", IEEE J. Emerg. Sel. Topics Power Electron., vol. 9, no. 1, pp. 702-715, Feb. 2021.
[18] K. Wang, Q. Gao, G. Wei and X. Yang, "Integrated fractional-turn planar transformer for MHz and high-current applications", IEEE Trans. Power Electron., vol. 38, no. 6, pp. 7374-7384, Jun. 2023.
[19] M. Xu, Y. Liu, J. Sun, and F. C. Lee, "Σ/sigma DC/DC conversion for computing and telecom applications," in Proc. IEEE Power Electron. Spec. Conf. (PESC), Rhodes, Greece, Jun. 2008, pp. 1190–1195.
[20] X. Wu, H. Chen and Z. Qian, "1-MHz LLC resonant DC transformer (DCX) with regulating capability", IEEE Trans. Ind. Electron., vol. 63, no. 5, pp. 2904-2912, May 2016.
[21] T. Liu, Y. Han, X. Wu, S. Yang, and G. Xie, "A MHz regulated DC transformer with wide voltage range," in Proc. IEEE Int. Power Electron. Appl. Conf. Expo. (PEAC), Shenzhen, China, Nov. 2018, pp. 794–797.
[22] T. Liu, X. Wu and S. Yang, "1 MHz 48–12 V regulated DCX with single transformer", IEEE J. Emerg. Sel. Topics Power Electron., vol. 9, no. 1, pp. 38-47, Feb. 2021.
[23] T. Liu, T. Huang and X. Wu, "High-Efficiency High-Density RDCX Modules Cascaded with CHB PFC Stage," 2023 IEEE 2nd International Power Electronics and Application Symposium (PEAS), Guangzhou, China, 2023, pp. 107-110.
[24] H. Chiu, Y. Lo, P. Tseng, and Y. Liu, "High-efficiency battery charger with cascode output design," IET Power Electron., vol. 7, no. 7, pp. 1725-1735, Jul. 2014.
[25] G. Fan, X. Wu, T. Liu and Y. Xu, "High-Efficiency High-Density MHz Cellular DC/DC Converter for On-Board Charger," IEEE Trans. Power Electron., vol. 37, no. 12, pp. 15666-15677, Dec. 2022.
[26] C. Wang, M. Li, Z. Ouyang and G. Wang, "Resonant Push–Pull Converter with Flyback Regulator for MHz High Step-Up Power Conversion," IEEE Trans. Ind. Electron., vol. 68, no. 2, pp. 1178-1187, Feb. 2021.
[27] J. A. Carrasco, A. H. Weinberg, E. Maset and E. J. Dede, "A high-efficiency regulation technique for a zero-voltage zero-current power switching converter", IEEE Trans. Power Electron., vol. 13, no. 4, pp. 739-747, Jul. 1998.
[28] J. M. Blanes, A. Garrigos, J. A. Carrasco, J. Ejea-Martí and E. Sanchis-Kilders, "High-efficiency regulation method for a zero-current and zero-voltage current-fed push–pull converter", IEEE Trans. Power Electron., vol. 26, no. 2, pp. 444-452, Jul. 2011.
[29] Y. Cao, M. Ngo, R. Burgos, A. Ismail and D. Dong, "Switching transition analysis and optimization for bidirectional CLLC resonant DC transformer", IEEE Trans. Power Electron., vol. 37, no. 4, pp. 3786-3800, Apr. 2022.
[30] Q. Zhu, L. Wang, L. Zhang and A. Q. Huang, "A 10 kV DC transformer (DCX) based on current fed SRC and 15 kV SiC MOSFETs", Proc. IEEE Appl. Power Electron. Conf. Expo., pp. 149-155, 2018.
[31] W. Qin, X. Wu and J. Zhang, "A Family of DC Transformer (DCX) Topologies Based on New ZVZCS Cells with DC Resonant Capacitance," IEEE Trans. Power Electron., vol. 32, no. 4, pp. 2822-2834, Apr. 2017.
[32] S. Rivera et al., "Partial-power converter topology of type II for efficient electric vehicle fast charging", IEEE J. Emerg. Sel. Topics Power Electron., vol. 10, no. 6, pp. 7839-7848, Dec. 2022.
[33] M. Daryaei, M. Esteki and S. A. Khajehoddin, "High efficiency and full MPPT range partial power processing PV module-integrated converter", IEEE Trans. Power Electron., vol. 38, no. 5, pp. 6627-6641, May 2023.
[34] P. Granello, T. B. Soeiro, N. H. van der Blij and P. Bauer, "Revisiting the partial power processing concept: Case study of a 5-kW 99.11% efficient flyback converter-based battery charger", IEEE Trans. Transport. Electrific., vol. 8, no. 3, pp. 3934-3945, Sep. 2022.
[35] M. Li, Z. Ouyang and M. A. E. Andersen, "A hybrid multitrack-sigma converter with integrated transformer for wide input voltage regulation", Proc. IEEE Appl. Power Electron. Conf. Expo. (APEC), pp. 1844-1850, Dec. 2020.
[36] M. Kasper, D. Bortis, G. Deboy, and J. W. Kolar, "Design of a highly efficient (97.7%) and very compact (2.2 kW/dm3) isolated AC–DC telecom power supply module based on the multicell ISOP converter approach," IEEE Trans. Power Electron., vol. 32, no. 10, pp. 7750–7769, Oct. 2017.